J. Phys.: Condens. Matter **24** (2012) 255402 (7pp) doi:10.1088/0953-8984/24/25/255402

Lattice dynamics of $FeSb_2$

N Lazarević[1], M M Radonjić[2], D Tanasković[2], Rongwei Hu[3,4], C Petrovic[3] and Z V Popović[1]

[1] Center for Solid State Physics and New Materials, Institute of Physics Belgrade, University of Belgrade, Pregrevica 118, 11080 Belgrade, Serbia
[2] Scientific Computing Laboratory, Institute of Physics Belgrade, University of Belgrade, Pregrevica 118, 11080 Belgrade, Serbia
[3] Condensed Matter Physics and Materials Science Department, Brookhaven National Laboratory, Upton, NY 11973-5000, USA

E-mail: nenad.lazarevic@ipb.ac.rs

Received 20 March 2012, in final form 30 April 2012
Published 28 May 2012
Online at stacks.iop.org/JPhysCM/24/255402

Abstract
The lattice dynamics of $FeSb_2$ is investigated by first-principles density functional theory calculations and Raman spectroscopy. All Raman- and infrared-active phonon modes are properly assigned. The calculated and measured phonon energies are in good agreement. We have observed strong mixing of the A_g symmetry modes, with the intensity exchange in the temperature range 210 and 260 K. The A_g mode repulsion increases by doping $FeSb_2$ with Co, with no signatures of the electron–phonon interaction for these modes.

(Some figures may appear in colour only in the online journal)

1. Introduction

$FeSb_2$ is a strongly correlated narrow-gap semiconductor which has recently attracted a lot of attention due to its unusual thermoelectric properties [1–6]. It was shown that $FeSb_2$ has colossal thermopower S at 10 K (in the range from 1 to 45 mV K^{-1} [5, 7]) and the largest power factor $S^2\sigma$ ever reported [5, 7–9]. The phonon contribution to S remains controversial [10]. Also, the thermal conductivity κ of $FeSb_2$ is relatively high and, at around 10 K, is dominated by the phonons [5]. Consequently, full knowledge of $FeSb_2$ lattice dynamics is necessary in order to understand the low temperature transport and thermodynamic properties of this material.

The infrared-active phonon frequencies of $FeSb_2$ were obtained from the polarized far-infrared reflectivity spectra [11]. From $E \parallel b$ polarized reflectivity measurements on the (102) plane of $FeSb_2$ single crystal, Perucchi *et al* observed four modes at 106.4, 231, 257 and 271 cm^{-1} at 10 K (factor group analysis predicts three B_{2u} modes for this polarization configuration). For $E \perp b$ polarization, both B_{1u} and B_{3u} symmetry modes can be observed from the (102) plane. Three (of four) modes at 121, 216 and 261.4 cm^{-1} are observed for this polarization. Raman scattering measurements on $FeSb_2$ were published in [12–15]. Lutz and Müller [12] observed two Raman-active modes at about 175 and 154 cm^{-1} on hot-pressed samples, and assigned them as the A_g symmetry modes. In contrast, Racu *et al* [13] observed three Raman modes at about 150, 157 and 180 cm^{-1} using polarized Raman scattering measurements on $FeSb_2$ single crystals and assigned them as the B_{1g}, A_g and B_{1g} symmetry modes, respectively. Finally, all six Raman-active modes of $FeSb_2$ predicted by the factor group analysis ($2A_g+2B_{1g}+B_{2g}+B_{3g}$) were observed in [14]. Polarized Raman scattering spectra of the $Fe_{1-x}M_xSb_2$ (M = Cr, Co) single crystals was studied in [15]. The linewidths and energies of the Raman modes were analyzed as a function of doping x and temperature. A strong electron–phonon interaction, observed for the B_{1g} symmetry mode of pure $FeSb_2$, produces significant mode asymmetry. The electron–phonon interaction is drastically reduced with increasing concentration of Co and Cr in $Fe_{1-x}(Co, Cr)_xSb_2$. The mixing of the A_g symmetry phonon modes has been observed both in pure and Cr-doped samples [15].

In this paper we report an *ab initio* study of the lattice dynamics of $FeSb_2$. The calculated phonon energies at the Γ-point are in good agreement with experimental data. The phonon density of state shows a gap at about 175 cm^{-1}, which divides a low frequency region, where vibration modes are mostly Raman-active, from a high frequency region, where only infrared-active modes appear. The calculated phonon dispersions for two A_g symmetry modes indicate

[4] Present address: Department of Physics, University of Maryland, College Park, MD 20742-4111, USA.

strong mode mixing. This is indeed observed in our polarized Raman scattering spectra. The A_g mode intensity exchange in the temperature range between 210 and 260 K agrees well with theoretical calculations, excluding any additional temperature-dependent electron–phonon coupling for these modes. The mode repulsion increases with Co doping.

2. Experiment

Single crystals of $FeSb_2$ and $Fe_{0.75}Co_{0.25}Sb_2$ were grown by the self-flux method and characterized as described elsewhere [1]. The Raman scattering measurements were performed using a Jobin Yvon T64000 Raman system in the micro-Raman configuration. The 514.5 nm line of an Ar^+/Kr^+ mixed gas laser was used as an excitation source. Focusing of the laser beam was realized with a long distance microscope objective (magnification 50×). We have found that a laser power level of 0.02 mW on the sample is sufficient to obtain the Raman signal and, except for the signal-to-noise ratio, no changes of the spectra were observed as a consequence of laser heating by further lowering the laser power. The corresponding excitation power density was less than 0.1 kW cm^{-2}. Low temperature measurements were performed between 15 and 300 K using a KONTI CryoVac continuous helium flow cryostat with a 0.5 mm thick window. Raman scattering measurements of pure and Co-doped $FeSb_2$ samples were performed using the $(10\bar{1})$-oriented $FeSb_2$ samples. Selection rules for parallel and crossed polarization from the $(10\bar{1})$ plane of the orthorhombic crystal symmetry and the mode assignment have been presented in [14].

3. Numerical method

$FeSb_2$ crystallizes in the orthorhombic marcasite-type structure of the centrosymmetric *Pnnm* (D_{2h}^{12}) space group, with two formula units ($Z = 2$) per unit cell [16, 17]. The basic structural unit is built up of Fe atoms surrounded by deformed Sb octahedra. These structural units are corner-sharing in the (*ab*) plane and edge-sharing along the *c* axis. Two Fe atoms are in (2a) Wyckoff positions at (0, 0, 0) and four Sb atoms are in (4g) Wyckoff positions at (0, u, v) of the *Pnnm* space group. Our density functional theory (DFT) calculations are performed within the generalized gradient approximation (GGA) with the PW91 exchange–correlation functional which is used to calculate ultra-soft pseudopotentials [18], as implemented in the QUANTUM ESPRESSO package [19]. The iron (antimony) pseudopotential takes into account $3s^23p^64s^23d^6$ ($4d^{10}5s^25p^3$) electron states for the valence electrons. The Brillouin zone was sampled with an 8 × 8 × 8 Monkhorst–Pack **k**-space mesh and with the Marzari–Vanderbilt cold smearing (0.005 Ryd) [20]. The obtained optimized structural parameters are $a = 5.859$ Å, $b = 6.583$ Å, $c = 3.812$ Å, $u = 0.1882$ and $v = 0.3554$, which are in good agreement with the experiment. Our band structure calculations agree well with those previously reported [10, 21, 22].

4. Results and discussion

The lattice dynamics is investigated by the density functional perturbation theory (DFPT) [23] within the theory of linear response. This method includes calculations of charge response to the lattice distortions (allowed by the symmetry operations) for the specified vectors in the first Brillouin zone. Calculations start from the previously calculated ground state atomic and electronic configuration and continue with the self-consistent calculations of the charge response for each different displacement. The normal modes of the optically active phonons (at the Γ-point) are given in figure 1. Because Fe ions are located in the center of inversion of the *Pnnm* space group, they do not contribute to the Raman scattering process, i.e. the Raman modes of $FeSb_2$ originate only from the Sb atom vibrations, in a manner illustrated in figure 1. In the case of infrared-active modes, both the Fe and Sb atoms contribute to the normal modes, see figure 1.

In order to obtain the phonon dispersion curves, we have calculated the phonon frequencies at the 4 × 4 × 4 Monkhorst–Pack *q*-point mesh and interpolated along the chosen path. Figure 2(a) shows the calculated phonon dispersions, whereas figure 2(b) represents the phonon density of states of $FeSb_2$. It is interesting to note that there is a frequency gap in the phonon dispersion of $FeSb_2$ at about 175 cm^{-1}. The lower frequency range is dominated by Sb atom vibrations (mostly Raman-active vibrations), whereas the Fe atoms vibrate at frequencies higher than 175 cm^{-1}. These modes are only infrared-active.

The phonon density of states peaked structure between 50 and 90 cm^{-1} corresponds to the low frequency acoustic modes associated with the low-lying B_{2g} Raman-active mode, whose calculated frequency is at 89.4 cm^{-1}. Sharp peaks in the phonon density of states above 90 cm^{-1} come from the flat regions of the dispersion curves of the corresponding Raman (below 175 cm^{-1}) and infrared (above 175 cm^{-1}) modes.

The lattice dynamics calculations allow us to assign the infrared-active modes, experimentally observed in [11]. The assignment of the infrared-active modes is done according to the mode energy and symmetry. As we have already mentioned, for $E \parallel b$ (B_{3u} symmetry modes) four modes are observed [11] instead of three. We believe that the appearance of two modes at about 257 and 271 cm^{-1} instead of a single frequency mode is a consequence of the splitting of a relatively broad oscillator (whose calculated TO frequency is 259.6 cm^{-1}), due to anharmonicity effects [24]. The B_{1u} infrared-active mode of $FeSb_2$ is recently observed at 195 cm^{-1} in [25]. The frequencies and assignment of all infrared-active modes are given in table 1.

The DFT calculations are performed at zero temperature and should be matched with the phonon energies at zero temperature. For this purpose, we have analyzed the change of the Raman mode energy and linewidth with temperature, induced by the anharmonicity effect.

Having in mind the total absence of the gap between acoustic and Raman-active phonons in the phonon DOS, the influence of the anharmonic effects on the Raman mode

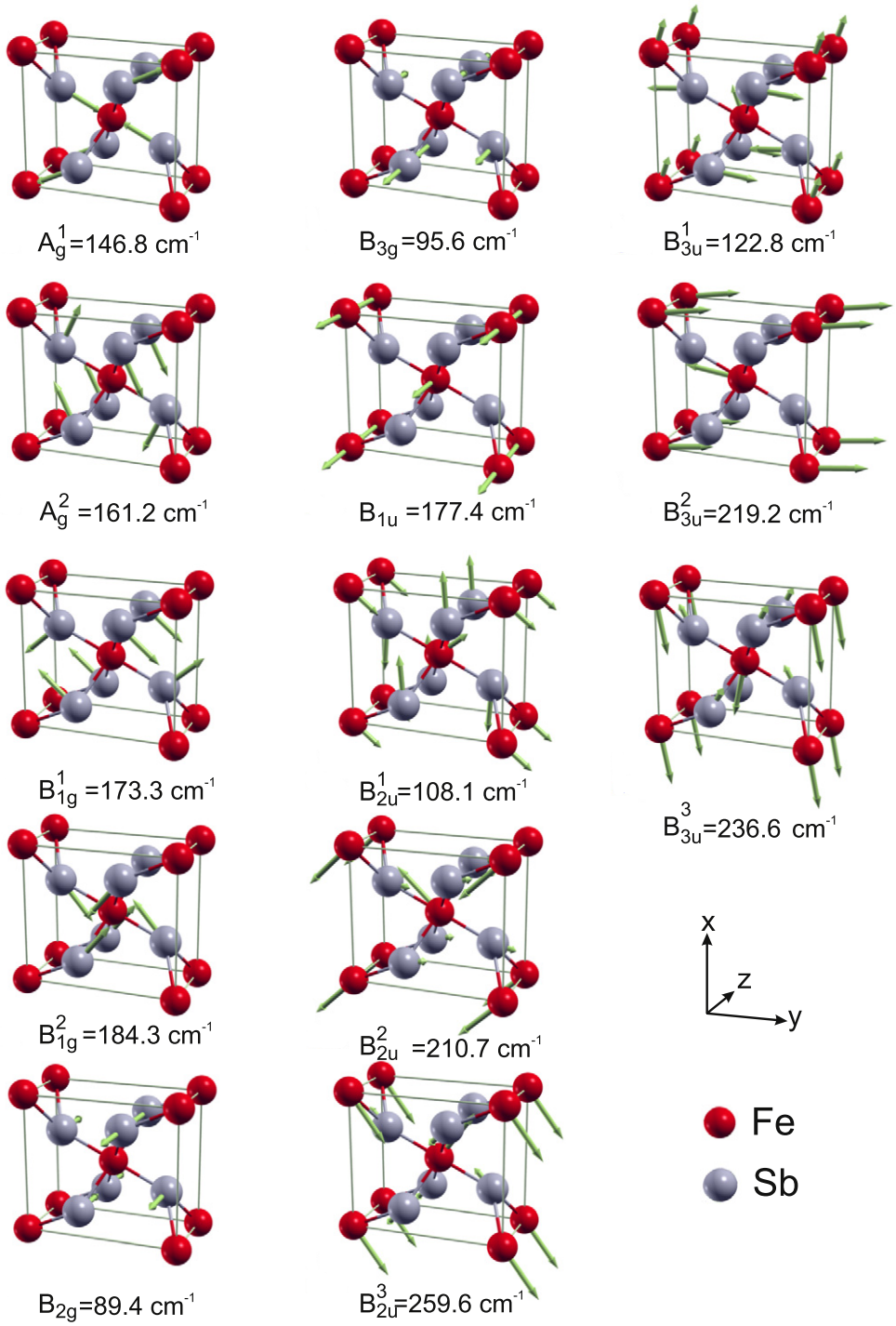

Figure 1. Atomic displacement patterns for the vibrational modes of $FeSb_2$. The lengths of the arrows are proportional to the square root of the vibration amplitudes.

energy can be taken into account via three- and four-phonon processes by applying Klemens's ansatz [26, 27]:

$$\begin{aligned}\Omega(T) &= \Omega_0 - \Delta^{(3)}(T) - \Delta^{(4)}(T),\\ \Delta^{(3)}(T) &= C\left(1 + \frac{2}{e^x - 1}\right),\\ \Delta^{(4)}(T) &= D\left(1 + \frac{3}{e^y - 1} + \frac{3}{(e^y - 1)^2}\right),\end{aligned} \tag{1}$$

where Ω_0 is the temperature-independent contributions to the Raman mode energy, C (D) is the three (four)-phonon anharmonic constant, $x = \hbar\Omega_0/2k_BT$ and $y = \hbar\Omega_0/3k_BT$.

There are two main contributions to the phonon linewidth: (i) anharmonic decay of the phonon and (ii) perturbation of the translational symmetry of the crystal by the presence of impurities and defects. Having this in mind, the phonon linewidth can be described with

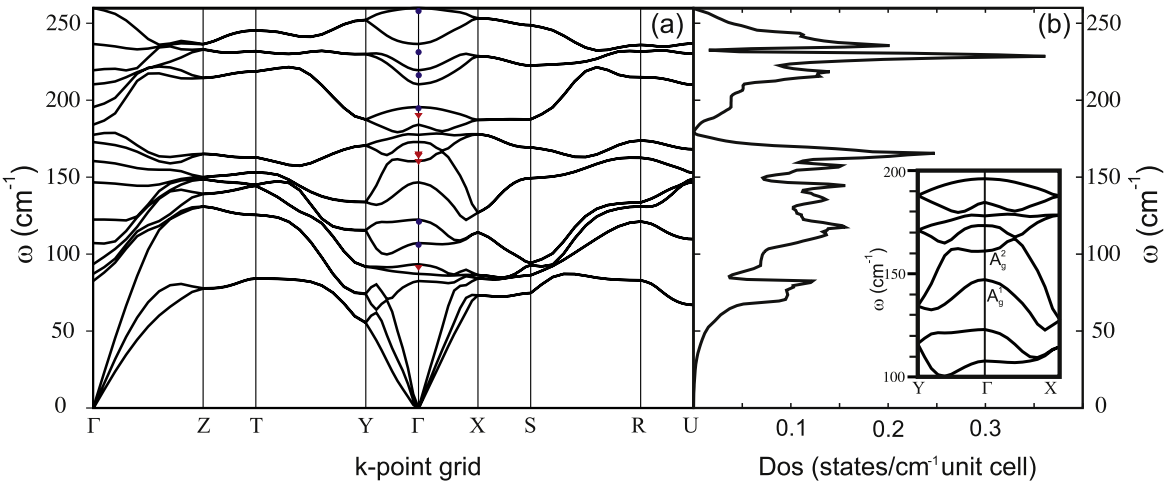

Figure 2. Phonon dispersion (a) and phonon density of states (b) for $FeSb_2$. Triangles and circles represent experimentally observed Raman and infrared mode energies. Inset: dispersion curves of A_g phonon modes along the Γ–Y and Γ–X directions.

Table 1. Raman- and infrared-active mode energies (in cm^{-1}) of $FeSb_2$ single crystal.

Symmetry	Exp. [14]	Ω(0)	Calculation	Activity	Symmetry	Exp. [11, 25]	Calculation	Activity
A_g^1	150.7	160.3	146.8	R	B_{1u}	195	177.4	IR
A_g^2	153.6	164.4	161.2	R	B_{2u}^1	106.4	108.1	IR
B_{1g}^1	154.3	164.6	173.3	R	B_{2u}^2	231.0	210.7	IR
B_{1g}^2	173.9	190.4	184.3	R	B_{2u}^3	257.0	259.6	IR
B_{2g}	90.4		89.4	R		271.0		IR
B_{3g}	151.7		95.6	R	B_{3u}^1	121.0	122.8	IR
					B_{3u}^2	216.0	219.2	IR
					B_{3u}^3	261.4	236.6	IR
					A_u^1		84.9	Silent
					A_u^2		195.2	Silent

$$\Gamma(T) = \Gamma_0 + \Gamma^{(3)}(T) + \Gamma^{(4)}(T),$$
$$\Gamma^{(3)}(T) = A\left(1 + \frac{2}{e^x - 1}\right), \qquad (2)$$
$$\Gamma^{(4)}(T) = B\left(1 + \frac{3}{e^y - 1} + \frac{3}{(e^y - 1)^2}\right),$$

where Γ_0 is the temperature-independent linewidth, which originates mainly from (ii), and A (B) is the three (four)-phonon anharmonic constant. Analysis of energy and FWHM (full width at half-maximum) versus temperature for the B_{1g}^1 mode is presented in figure 3. Because anharmonicity constant ratios B/A and D/C are very small, see figure 3, the contribution of the four-phonon processes is small compared to that of the three-phonon processes. The obtained value of $\Omega(0) = 164.6$ cm^{-1} for this mode at zero temperature is in good agreement with the DFT results. Similar analyses have been performed for the B_{1g}^2 symmetry mode giving the value of $\Omega(0) = 190.4$ cm^{-1} at zero temperature [15], which is in rather good agreement with our calculations.

The calculated energy (89.4 cm^{-1}) for the B_{2g} symmetry mode at the Γ-point shows excellent agreement with the room temperature experimental data. This is to be expected since low energy modes show weak anharmonicity effects. A surprisingly large discrepancy between experimental and calculated phonon energies is observed for the B_{3g} mode. Since the B_{2g} and B_{3g} modes represent the same type of vibrations, the chain rotation around the x and y axis, respectively (see figure 1), their frequencies should be very close. This large disagreement is also unexpected since all other calculated phonon energies show rather good agreement with the experimentally obtained data. By detailed inspection of our previously published Raman spectra [14] of pure, Co- and Cr-doped $FeSb_2$ samples we did not find any mode in a low frequency region close to the calculated frequency (95 cm^{-1}) for the B_{3g} mode. The missing B_{3g} mode is most probably of very low intensity and it was not possible to extract it from the noise. The mode observed at 151.7 cm^{-1} for $(x'y)$ polarization, which we assigned in [14] as the B_{3g} mode, could be the 'leakage' of the A_g^1 mode, which appears at about 150.7 cm^{-1} in the $(x'x')$ polarization.

It is interesting to note that the dispersion curves of two A_g symmetry Raman modes have opposite slopes near the Γ-point (see the inset of figure 2(b)), which leads to the mode mixing with the 'anticrossing' effect. The A_g^1 mode represents the stretching vibration of Sb ions, whereas the A_g^2 mode represents twisting of Sb ions, which tends to rotate Sb ions

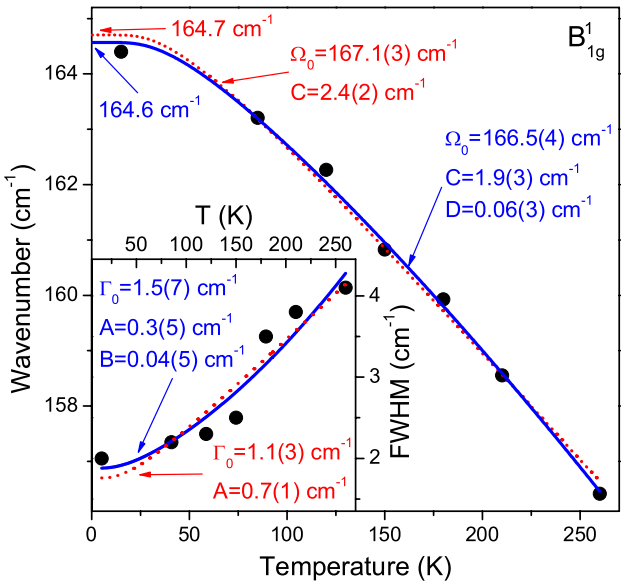

Figure 3. B^1_{1g} mode wavenumber as a function of temperature. Solid line represents theoretical extrapolation by using equation (1), whereas dashed line represent theoretical extrapolation obtained by omitting the four-phonon contribution in equation (1). Inset: theoretical calculation of FWHM obtained by using equation (2) (solid line) and by omitting the four-phonon contribution in equation (2) (dashed line).

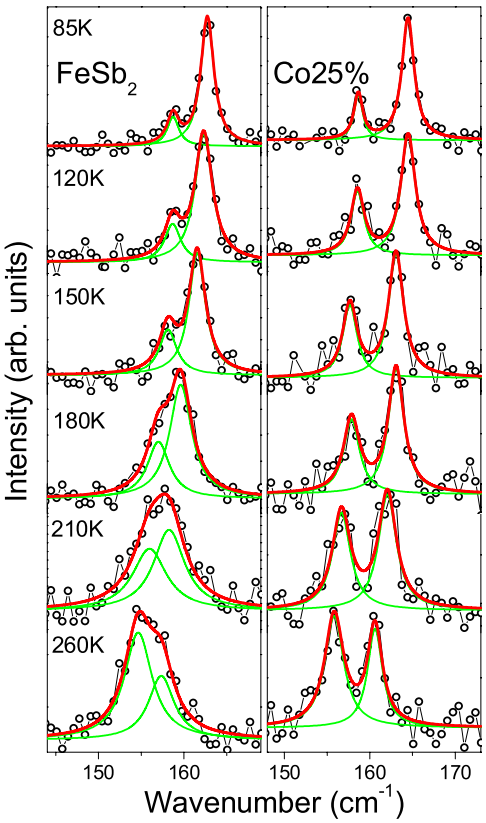

Figure 4. The Raman scattering spectra of $FeSb_2$ (left panel) [15] and $Fe_{0.75}Co_{0.25}Sb_2$ (right panel) single crystals in the $(x'x')$, $x' = \frac{1}{\sqrt{2}}[101]$ configuration (A_g symmetry modes) measured at various temperatures.

around the z axis, see figure 1. In our previous paper [15], we showed the existence of the A_g mode mixing in the case of pure $FeSb_2$ and Cr alloyed samples. Here we present a detailed analysis of the mixing of two A_g modes for pure and 25% Co alloyed samples.

The polarized Raman scattering spectra for pure $FeSb_2$ (left panel [15]) and $Fe_{0.75}Co_{0.25}Sb_2$ (right panel) single crystals, measured in the $(x'x')$ configuration (A_g modes) at different temperatures, are presented in figure 4. The Lorentzian lineshape profile has been used for the extraction of mode energy and linewidth. Figure 5 shows the energies and normalized intensities as a function of temperature of the A_g modes for $FeSb_2$ and $Fe_{0.75}Co_{0.25}Sb_2$ single crystals. In the observed temperature range, energies of two A_g modes for pure and 25% Co-doped samples are very close, which implies the existence of mode mixing, manifested by mode repulsion and intensity transfer with the change of temperature [28]. Indeed, intensities of these modes are exchanged for both samples in the temperature range between 210 and 260 K (see figures 4 and 5).

In general, two phonon branches or any other elementary excitations of the same symmetry may couple, leading to the renormalization of the quasiparticle energies. Coupling between two phonon branches leads to the energy and linewidth changes (anticrossing effect). We can consider the coupling of two phonon branches as coupling of two quantum oscillators. When the perturbation is small, we can write the Hamiltonian of the system as

$$\hat{H} = \begin{bmatrix} \Omega_1(T) & V \\ V & \Omega_2(T) \end{bmatrix}, \qquad (3)$$

where V is the interaction constant, and $\Omega_1(T)$ and $\Omega_2(T)$ are the unperturbed mode energies, obtained by taking into account, due to simplicity, only three-phonon processes in equation (1). The eigenvalues of the Hamiltonian give a rather good fit of the experimental data (solid lines in figures 5(a) and (b)), suggesting the absence of any additional temperature-dependent couplings (i.e. electron–phonon interaction) for these modes. Fitting parameters are presented in table 2. Zero-temperature energies of A^1_g and A^2_g symmetry modes, in the absence of interaction, for a pure (25% Co-doped) sample are $\Omega_1(0) = 160.3$ cm^{-1} and $\Omega_2(0) = 164.5$ cm^{-1} ($\Omega_1(0) = 161.1$ cm^{-1} and $\Omega_2(0) = 165.3$ cm^{-1}). One can notice that the zero-temperature energies for decoupled modes are increased by 0.8 cm^{-1} (about 0.5% increase) with 25% Co doping, corresponding to the unit cell volume contraction [3]. The phonon energy of the bond-stretching mode scales as R^{-3}, where R is the bond length [29]. Since the change in R^{-3} is proportional to the inverse volume change, we can expect the phonon-energy change for bond-stretching modes (A_g modes) to be inversely proportional to the volume change. Because the Co atom substitutes the Fe atom, which is located in the center of the inversion, there is no change in Raman spectra due to the mass effect. Additional energy separation between the coupled modes is caused by the interaction. With Co doping, the interaction constant V increases, resulting in larger mode separation for the 25% doped sample.

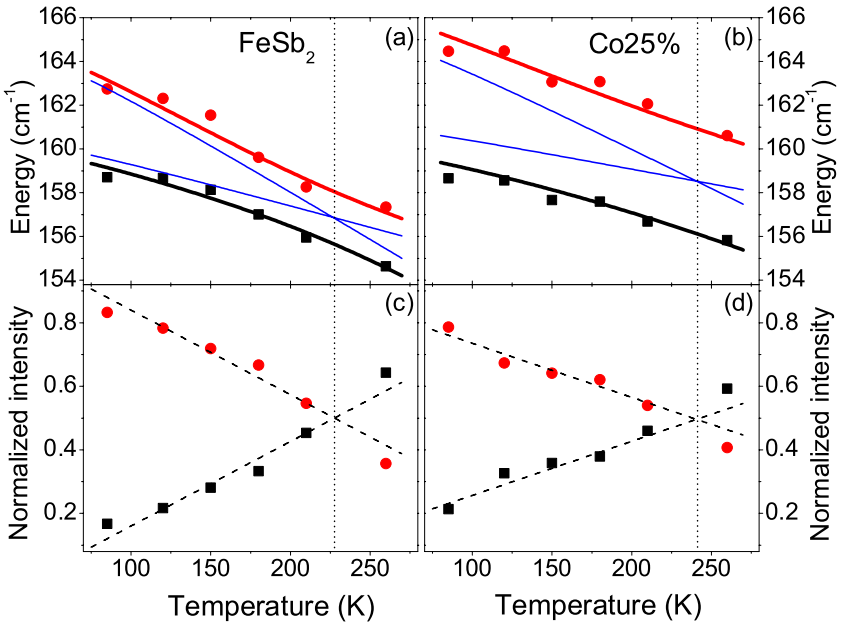

Figure 5. Energies (a), (b) and normalized intensities (c), (d) as a function of temperature of the A_g modes for $FeSb_2$ and $Fe_{0.75}Co_{0.25}Sb_2$ single crystals. Thin solid lines show energy versus temperature dependence of the A_g modes without coupling. Thick solid lines (red and black) show mode energy–temperature dependence for two coupled A_g modes calculated using equation (3). The dashed lines are guides for the eyes.

Table 2. Best fit parameters for energy–temperature dependence of the A_g symmetry modes using equation (3).

Compound	Symmetry	Ω_0 (cm^{-1})	C (cm^{-1})	V (cm^{-1})
$FeSb_2$	A_g^1	167.1	2.65	1.2
	A_g^2	161.5	1.16	
$Fe_{0.75}Co_{0.25}Sb_2$	A_g^1	167.5	2.2	2.4
	A_g^2	161.9	0.80	

5. Conclusion

In summary, we presented a detailed theoretical and experimental study of the $FeSb_2$ phonon dynamics. All experimentally observed Raman- and infrared-active modes were successfully assigned. The calculated phonon frequencies at the Γ-point agree with the measured frequencies. We believe that the low energy B_{3g} mode is of a very low intensity and therefore is not observed in the Raman experiments. The phonon mode at 150.7 cm^{-1}, which we previously assigned as the B_{3g} mode, could be the 'leakage' of the A_g^1 mode. The strong intensity exchange of the A_g symmetry modes, observed in our Raman scattering experiments in the temperature range between 210 and 260 K, is successfully described by a simple model of coupling of two phonon branches with the same symmetry. The mode mixing is also implied from the calculated dispersion curves, which show opposite slopes for two A_g modes near the Γ-point. We find that doping of $FeSb_2$ with Co increases the A_g mode repulsion.

Acknowledgment

This work was supported by the Serbian Ministry of Education and Science under projects ON171032, III45018 and ON171017. Part of this work (CP and RH) was carried out at the Brookhaven National Laboratory which is operated for the Office of Basic Energy Sciences, US Department of Energy by Brookhaven Science Associates (DE-Ac02-98CH10886). Numerical simulations were run on the AEGIS e-Infrastructure, supported in part by FP7 projects EGI-InSPIRE, PRACE-1IP and HP-SEE. ZVP and MMR acknowledges support from the Swiss National Science Foundation through the SCOPES grant no. IZ73Z0-128169.

References

[1] Petrovic C, Kim J W, Bud'ko S L, Goldman A I, Canfield P C, Choe W and Miller G J 2003 *Phys. Rev.* B **67** 155205
[2] Petrovic C, Lee Y, Vogt T, Lazarov N D, Bud'ko S L and Canfield P C 2005 *Phys. Rev.* B **72** 045103
[3] Hu R, Mitrović V F and Petrovic C 2006 *Phys. Rev.* B **74** 195130
[4] Hu R, Mitrović V F and Petrovic C 2007 *Phys. Rev.* B **76** 115105
[5] Bentien A, Johnsen S, Madsen G K H, Iversen B B and Steglich F 2007 *Europhys. Lett.* **80** 39901
[6] Hu R, Mitrović V F and Petrovic C 2008 *Appl. Phys. Lett.* **92** 182108
[7] Sun P, Oeschler N, Johnsen S, Iversen B B and Steglich F 2010 *Dalton Trans.* **39** 1012
[8] Sun P, Oeschler N, Johnsen S, Iversen B B and Steglich F 2009 *Phys. Rev.* B **79** 153308
[9] Takahashi H, Yasui Y, Terasaki I and Sato M 2011 *J. Phys. Soc. Japan* **80** 054708
[10] Tomczak J M, Haule K, Miyake T, Georges A and Kotliar G 2010 *Phys. Rev.* B **82** 085104

[11] Perucchi A, Degiorgi L, Hu R, Petrovic C and Mitrović V F 2006 *Eur. Phys. J.* B **54** 175
[12] Lutz H D and Müller B 1991 *Phys. Chem. Miner.* **18** 265
[13] Racu A M, Menzel D, Schoenes J, Marutzky M, Johnsen S and Iversen B B 2008 *J. Appl. Phys.* **103** 07C912
[14] Lazarević N, Popović Z V, Hu R and Petrovic C 2009 *Phys. Rev.* B **80** 014302
[15] Lazarević N, Popović Z V, Hu R and Petrovic C 2010 *Phys. Rev.* B **81** 144302
[16] Holseth H and Kjekshus A 1968 *Acta Chem. Scand.* **22** 3273
[17] Holseth H, Kjekshus A and Andresen A F 1970 *Acta Chem. Scand.* **24** 3309
[18] www.quantum-espresso.org/pseudo.php
[19] Giannozzi P *et al* 2009 *J. Phys.: Condens. Matter* **21** 395502
[20] Marzari N, Vanderbilt D, De Vita A and Payne M C 1999 *Phys. Rev. Lett.* **82** 3296
[21] Lukoyanov A V, Mazurenko V V, Anisimov V I, Sigrist M and Rice T M 2006 *Eur. Phys. J.* B **53** 205
[22] Bentien A, Madson G K H, Johnsen S and Iversen B B 2006 *Phys. Rev.* B **74** 205105
[23] Baroni S, de Gironcoli S, Dal Corso A and Giannozzi P 2001 *Rev. Mod. Phys.* **73** 515
[24] Gervais F and Piriou B 1974 *Phys. Rev.* B **10** 1642
[25] Herzog A, Marutzky M, Sichelschmidt J, Steglich F, Kimura S, Johnsen S and Iversen B B 2010 *Phys. Rev.* B **82** 245205
[26] Balkanski M, Wallis R F and Haro E 1983 *Phys. Rev.* B **28** 1928
[27] Klemens P G 1966 *Phys. Rev.* **148** 845
[28] Iliev M N, Abrashev M V, Laverdire J, Jandl S, Gospodinov M M, Wang Y-Q and Sun Y-Y 2006 *Phys. Rev.* B **73** 064302
[29] Popović Z V, Stergiou V, Raptis Y S, Konstantinović M J, Isobe M, Ueda Y and Moshchalkov V V 2002 *J. Phys.: Condens. Matter* **14** L583